ISSN: 2349-5197
Impact Factor: 3.765

INTERNATIONALJOURNALOFRESEARCH SCIENCE& MANAGEMENT

DESIGN OF SOLAR PHOTOVOLTAIC MICRO-POWER SUPPLY FOR APPLICATION OF WIRELESS SENSOR NODES IN SIMPLE ILLUMINATION ENVIRONMENTS

Abir Kessebi, Pr.Bahri Rezig
University of Tunis El Manar, ENIT. LPMS 1002, Tunisia

DOI: 10.5281/zenodo.1291886

Keywords: Boost converter, Dialux, Matlab, Power management, Wireless Sensor

Abstract

Nowadays, it can be observed that Wireless Sensors Networks (WSN) are taking increasingly vital roles in many applications. However, the main challenging issue with adopting WSN technology is the use of power sources such as batteries and supercapacitors, which have a limited lifetime. A smart solution that could tackle this problem is using ambient Energy Harvesting technology. This paper presents a WSN microsystem with indoor light power harvesting using photovoltaic (PV) cell. The indoor light is a remix of artificial and natural light simulated in an office in Tunisia. We have evaluated the amount of light, his availability and the power that the PV cell can provide to the WSN. The WSN average energy consumption was calculated using the Heinzelman model. Simulation studies confirm that a 30 cm2 PV cell can satisfy the need of a low duty cycle sensor Node. Finally we propose a power management design through harvesting hybrid indoor light. The approach is inspired by the use of the Fractional Open Circuit Voltage based Maximum Power Point tracking (MPPT) concept for sub mw PV cells. Three scenarios of boost converter (BC) were studied in this work, first scenario is a typical BC with an input capacitor, second scenario is a BC without an input capacitor, and third scenario is a direct connection. We focused on analyzing the state of charge (SoC) of the output capacitor in those three scenarios and also when varying the number of series connected PVcells. At conclusion the validated scenario is the one who gives a better stabilization of PV cell voltage around the MPP and a better SoC for the energy storage unit.

Introduction

The term iPV stands for all types of photovoltaic cell that operate under indoor conditions supplied by a mixed light. The power that a PV cell can collect from indoor provides 3 orders of magnitude lower than outdoor environment [1]. The photovoltaic technology can be used as a power source in any scale, ranging from applications of mW (or even less) up to MW power plants [2]. The main researches on iPV has focused on energy harvesting, storage and maximum power point tracking [3]. Indoor photovoltaic is a promising field specially for supplying low power electronic circuitry as wireless sensor networks (WSN) which have many applications field like industry, health care, commercial and residential applications. In the first section of this work, we study the characteristics of indoor natural and artificial light. This light can be transformed into electricity if it's considered as source for a PV module. The computation was made using the radiosity method to determine the light distribution inside the room taking into account the sky diffuse radiation and all surfaces reflections. We used DIALUX software to calculate the spatial distribution of incident light on all the walls and on the ceiling to define which wall is expected to host the iPV generator.

In the second section we have evaluated, using Matlab/Simulink simulations, the amount of average energy consumption in a WSN based on a clustering topology and predicted the optimal number of clusters in order to optimize the energy and also to study the cloud integration effects on lifetime and Energy time dependency. A dimensioning of a photovoltaic cell is presented in the third and last section knowing that much research on supplying WSN by iPV has been done and recently, several authors [4-5-6-7] have studied the feasibility of satisfying WSN power need by only recycling indoor light.

Maximum power point tracking (MPPT) technologies have often been used for solar power systems with output power higher than 100 mW. By implementing switching regulator-based MPPT techniques, the EHM will operate near its theoretical maximum power point and generates power close to its highest conversion efficiency. One major challenge in energy harvesting systems is how to implement this type of input power management circuit with minimum power consumption overhead. The conventional methods of MPPT cannot be directly adopted because their power consumption is beyond the power budget of the small EH system, in this paper we analyze and simulate the power management using three scenarios and comparing them.

Evaluation of Available Hybrid Light Amount to Supply the PV cell

1- Simulation Parameters.

In this work, we used principally two software, Dialux4.12 for indoor light simulation and Origin 2016 for the graphing and data analysis. The method that Dialux apply for the calculation is the so-called radiosity method. These calculation codes are able to predict the amount of light received by any point of a given working plane and from one or more sources installed on the ceiling of the room.

A. The room geophysical parameters

The case studied consist on an office room located on Tunis, Tunisia with a dimension 3.6mx5.4m, a 2.800 m Height, 36.83° on Latitude and 10.15°on the Longitude. The Orientation is 20 degree to the north. Reflexion degree Rho (maximum value in dialux 90%): ceiling 70%, walls 50% and ground 20%. Objects in the room are two windows, a door, a table, a chair and two desks. The glass transmission factor of the window is 90%.The office is occupied from 9AM to 5PM for professional activity. Besides the room geometry, other parameters are involved as reflection coefficients of the walls and furniture.

B. The light source technology and arrangements

A light-emitting diode (LED) is a semiconductor device that emits visible light when an electric current passes through it. The light is not particularly bright, but in most LEDs it is monochromatic, occurring at a single wavelength. The artificial light source used in this work is a matrix of ALTO 11200 W75 840 O2 Downlight LED, the dimensions of the LED lamp are (L x l x H): 0.065x0.065x0.08m.

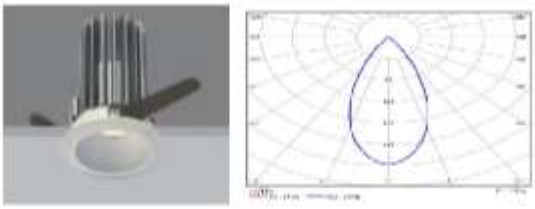

Fig.2. ALTO 11200 Light emission.

One Led power: 10 W
Luminous flow: 700 lm
The office is enlightened by 12 ALTO led on a straight disposition on the ceiling.
This disposition do satisfy the visual comfort for a professional activity on an office by 300 lux average light intensity on the working plan.

C. The active surface

The active surface is a surface on which the software will calculate either the amount of light intensity (lux) or the illuminance of the surface. The dimension, the surface origin position and the number of the calcul point are fixed by the user. In order to better study all of the office space, each wall contains an active surface. In our case, the active surface mesure 4 m2and contains 20 * 50 calculation point.

D. Tunisian Artificial Light Field evaluation

In recent years, there have been many new developments in the lighting industries, The Three major lamps type dominating are incandescent, fluorescent lamp and Light emitting diodes (LED). In Tunisia, in 2014 LED presents 39% of the total lamps used while incandescent represents 35% and Fluorescent 18%.

Table I. tunisian market share lighting technologies evolution from 1984 to 2014 [8].

Parc %	1984	1989	1994	1999	2004	2009	2014
Incandescent	83	79	76	73	68	55	35
Fluo	10	12	14	16	18	17	18
LCL*	0	0	0	0	3	19	39

LCL: low consumption lamp.

The contribution of LED lamp in the Tunisian Market due to its characteristics in energy saving do justify our choice of ALTO LED lamp in the first section.

2- Results: Simulated artificial light Distribution.

A Artificial light simulation Results

We carried out lighting simulations of an office building in order to clarify the characteristics of indoor lighting environments using Dialux.

The Led Lamp hanging on a 3.6mx5.4m area of the ceiling and oriented to the bottom. An active surface on each wall (1,2,3,4) is created to calculate the amount of light. Next we will compare the light intensity in different vertical active surface laid on every wall, for example we choose the wall 1 and 3.Light distribution is symmetric in wall 1 and 3. Both distributions are similar if we don't take into account the presence of any obstacle. The nonuniformity of light intensity on the active surface is similar to the shading phenomenon for a classic photovoltaic panel.

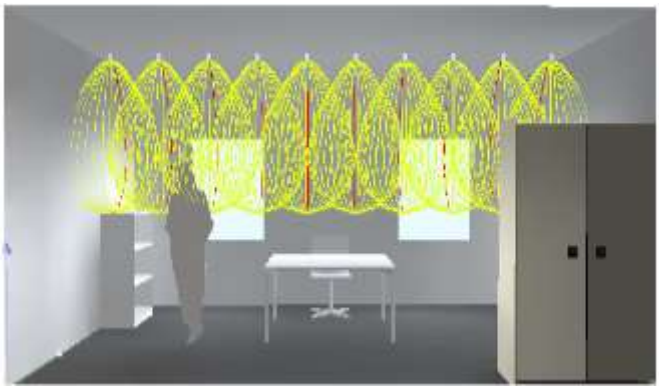

Fig.5. Artificial light lamp disposal

In table III is showing the photometric results generated by Dialux program for office considered.

Table III. artificial lighting: photometric results

surface	Medium luminance [lx]			Reflexing factor (%)	Medium luminaire [cd/m2]
	Direct	Indirect	Total		
Work plane	247	46	293	-	-
Floor	125	56	181	20	11
ceiling	0	55	55	70	12
Wall 1	100	36	136	50	22
Wall 2	101	48	149	50	24
Wall 3	0	63	63	50	10
Wall 4	74	49	124	50	20

3- Results: Indoor Natural Light Distribution

B Indoor Natural light simulation Results

The sky is divided into customizable luminous surfaces, which, depending on the sky model, location, date and time, a lighting density is affected. The natural light illuminance can also be calculated for many sky conditions like clear, overcast and partially overcast sky as shown in the next table.

Table V: The Average Illuminance Of Different Sky Situations

	Average illuminance on working plan (lux)	**Average illuminance on wall (lux)**
Clear sky	310	144
Partially overcast sky	450	120
Overcast sky	399	97

For natural light simulation, we have as input some parameters as the date 07/07/2015, time on 10h30 and the type of sky, we choose an overcast Sky. Table II shows levels of light intensity from the window side to the inner side on the working plane, ground, ceiling and walls.

Table vi. Photometric results for an overcast sky

Surfaces	ρ [%]	Emoy [lx]	Emin [lx]	Emax [lx]	Emin / Emoy
Working plane	/	455	43	3226	0.095
Ground	20	315	110	769	0.348
Ceiling	70	63	47	88	0.74
wall (4)	50	111	25	354	/

From version 4, Dialux is able to calculate the daylight. Calculation is based on the standard DIN 5034 and the publication of IEC 110.

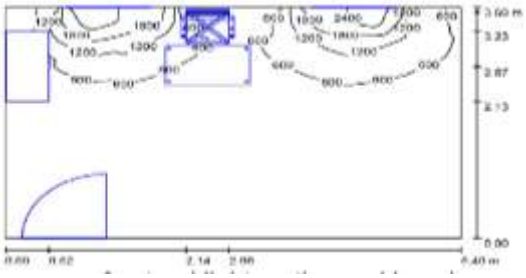

Fig.8. iso curve of natural light on the working plane

C Effect of location

Next table present indoor natural light simulation results for different locations.

Table vii. Effect of office location on indoor light intensity

	Working plan (lux)	*Ground (lux)*	*Wall (lux)*
Tunis	*294*	*181*	*114*
Sousse	*296*	*183*	*115*
Sfax	*298*	*184*	*115*
Tataouine	*304*	*188*	*116*

The increase of average light intensity, on the working plan ground or wall, when varying location can be contributed to approaching the south. The goal of the previous section is to simulate the amount of indoor light to supply a PV cell, Particular attention is paid to the important contribution of natural diffused light in Tunisia

to satisfy the load need. The realized simulations allow us to define the most appropriate location orientation and position to fix the solar cell and to know if the amount of the hybrid indoor light is sufficient to supply a node or not. In the worst case we will have 700 lux (200 lux of natural light in partially overcast sky and 500 lux of artificial light) and 800 lux in the best case (300 lux average light in Clear sky and 500 lux of artificial light), those photometric values should be converted into radiometric values when speaking of supplying a PV cell. The average incident light on the PV cell in the best location in the office correspond to 0.12 mW/cm2.

In next section, we review the models used to evaluate the energy consumption and lifetime in the case of a cluster-based WSN. We put a particular emphasis on conditions where energy consumption reduction and lifetime improvement are the most effective.

Wireless Sensor network Energy Consumption

1 Methodology

Wireless sensor networks (WSN) are more and more present In residential, commercial and industrial applications. In fact, they are found in intelligent buildings, in medicine and healthcare, agricultural control, logistics and many other fields. Moreover, the huge interest given recently to Internet of Things (IoT) is boosting the research on WSN. The major problem in WSN technology is energy supply. Indeed, batteries have a seriously limited capacity, need to be periodically replaced and are harmful to environment. Consequently, current research on wireless sensor network is focusing on reducing the total amount of energy consumption and extending the network lifetime [10]. Accurate estimation of sensor network lifetime requires, of course, an accurate energy consumption model. In this work, nodes are distributed according to a cluster-like distribution which is a commonly used topology. A node is randomly chosen to be a cluster head but it has to have the needed energy available. In the first sub-section, we present and put in coherence two energy consumption models: the first one (M. N. Halgamuge and al. 's model [11]) gives an expanded equation describing all the commonly used sensor functions, while the second model (Heinzelman et al. model [12]) focusses only on the most energy consuming part.

In the sub-second section, we report the simulation results where the crucial WSN parameters are studied like the distance to the base station, Duty cycle and number of clusters. This helped to study both network energy consumption and network lifetime.

Another way to analyze and explore energy and lifetime improvements is to integrate cloud. when integrating cloud into WSN, several shortfalls such as storage capacity of the data collecting together with data processing tasks on sensor nodes would become much easier [18] saving, by the way, the related energies. Such approach is developed in the third section.

In this work, we assume a network with N=100 immobile homogeneous nodes randomly distributed on 100x100 m2 area. Consider k the number of clusters in the network, in each cluster there are [(NK)-1] nodes and one Cluster Head (CH). CH's are special wireless nodes, with sufficient power available, which can send data to base station (BS) directly or via other CH's called CH-parents. Simple node senses physical signal and converts it to electrical signal. Signal conditioning and analog to digital conversion are also within node processing tasks [16]. Then, node transmits signals only to its related CH and not to BS. Each transmitted data message is fixed to b= 4000 bits long [14]. Figure (11) shows a network with a cluster tree topology: Each CH receives data from its own nodes or from other CH's called CH-children and transmits it to its CH-parent. a CH-parent can have many CH-children.

A. Communication Energy Dissipation Model (EDM)

Figure (12) presents a communication package mainly composed of the transmitter and the receiver circuits. It represents what is called the first order Radio Model. b is the number of bits per transmitted packet and d is distance between the sender and the receiver. Energy consumed to receive a b bit packet is expressed as follows:

$$ERx(b)=b.Eelec \quad (1)$$

to transmit a b bit data packet a node will consumes the following energy:

$$ETx(b,d) = b.Eelec + Eamp\ (b,d) \qquad (2)$$

Where:

Eelec is the energy dissipated per bit to run the transmitter or the receiver electrical circuit and Eamp (b,d) is the amplifier energy consumption, Moreover we have to count the power loss factor for free space fading (d2) or multipath fading (d4) depending on the distance, as follows:

$$E_{Tx}(b,d) = \begin{cases} (E_{elec}.b) + (.b.) \text{ if } d>d_o \\ (E_{elec}.b) + (\epsilon_{fs}.b), \text{ if } d<do \end{cases}$$

Where:

$$d_o = \qquad (4)$$

For the simulation described in this paper, we used typical radio parameter settings:
Eelec=50nj/bit, efs=10pj/bit/m2and emp=0.0013pj/bit/m and energy for data aggregation EDA = 5nJ/bit/signal [12].
Some models like M. N. Halgamuge et al. [16] consider the total energy consumed by the sensor as the sum of different specific energies as sensing, logging, micro-controller processing, radio transmitting and receiving, actuating and transient energy. The global network energy consumption equation is, then, given by:

$E_{tot} = k.\ E_{cluster}$

$$= b\left(N.E_{elec} + N.E_{proCH} + k.e_{mp}.d_{toBS}^{4} + k.E_{sensCH} + k.E_{tranCH} + k.E_{loggCH} + N.E_{elec} + N.e_{fs}\frac{M^2}{2\pi K} + N.E_{tranN} + N.E_{sensN} + N.E_{loggN}\right)$$

Where:
d_{toBS} is the distance from CH to the BS, and E_{proCH},E_{sensCH}, E_{tranCH}, E_{loggCH} are respectively processing, sensing, transient, logging energy in a CH and E_{tranN},Es_{ensN},E_{loggN} are respectively transient, sensing and logging energy in a node. Others, like Heinzelman and al. focus only on communication and computation components [17] [18] because they are the two prominent energy consumption tasks (about two thirds). We have adopted such a simplified expression to compute the total energy, considering the energy for data aggregation EDA as a constant.

Energy consumed by the network is the energy consumed in one cluster Ecluster multiplied by K total number of clusters.

$$E_{cluster} = E_{CH} + (\frac{N}{K} - 1)E_{non-CH}$$

$$E_{CH} = bE_{elec}(\frac{N}{K} - 1) + bE_{DA}.\frac{N}{K} + bE_{elec} + be_{mp}\,d_{toBS}^{4}$$

$$E_{non-CH} = bE_{elec} + be_{fs}\,d_{toCH}^{2}$$

If sensors are placed uniformly over a circle area than the mean square distance from a sensor to its CH is given by **[20]**:

$$d_{toCH}^{2} = \frac{M^2}{2\pi K}$$

Total energy per frame is:

$$E_{tot} = k.E_{cluster}$$

$$= b\,(N.E_{elec} + N.E_{DA} + k\, e_{mp}\, d_{toBS}^{4} + N.E_{elec} + N.e_{fs}\frac{M^2}{2\pi K}).$$

Several simulation environments for WSN does exist like GloMoSim/QualNet, OPNET, Modeler Wireless Suite, OMNeT++ and NS-2. The environment in which we carried out our simulation was Simulink MATLAB. Simulink provides a graphical user interface (GUI) for building models as block diagrams, using click-and-drag mouse operations [21] and It provides an interactive graphical environment and a customizable set of block libraries that facilities the designing, simulation, implementation, and testing a variety of systems[22].

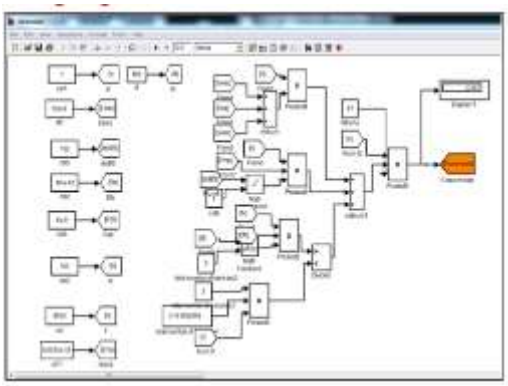

Figure.(13). Matlab/Simulink Simulation Model.

Table *VIII* contains Parameter values used in our simulated energy model:

Table VIII: parameters udes in the simulated energy model.

Symbol	*Description*	*Value*
Eelec	Energy dissipated in electronics	50nj/bit
N	Number of Nodes	100
b	Data packet size	4000 bits
emp	Multipath fading energy	0.0013pj/bit/m
d0	Threshold distance	
EDA	Energy for data aggregation	5nJ/bit/signal
efs	Free space fading energy.	10pj/bit/m2
M	Area surface	100*100M
TtrON	Time duration to transit from sleep to idle	2450 µs **[23]**
TtrOFF	Time duration to transit from idle to sleep	250 µs[**23]**
TA	Active time	1ms**[23]**
TS	Sleeping time	299 ms**[23]**
IA	Current: wakeup mode	8mA
IS	Current: sleeping mode	1. µA

B- LEACH protocol operations:
The time-line LEACH operations are composed principally of set-up phase and steady state phase. Into set-up phase, nodes organize themselves into clusters (all nodes Decide of Being CH, All CH send their position and approval request to the sink node, Scheduling all CH, all nodes are in listening to their CH, ALL nodes Decide to get associated to CH depending on the maximum power received [24].In the steady-state phase, node transmit data to their own CH in their assigned time slots. In each frame there are N number of data slots. Node i transmit its data during its time slot in each frame. Finally, All CH transmit aggregated data to the sink.

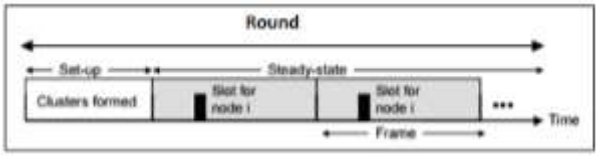

Figure.(14). Operations of LEACH protocol

In the previous section, the consumption of energy was calculated per frame although we have to express it per round.

$$E_{CH\ per\ round} = N_{frames\ per\ round} \times E_{CH\ per\ frame} \quad (8)$$

Simulations results are shown in next session.
The percentage of energy consumption per function were estimated in [11], communication has the biggest part by 51% from total WSN energy consumption, processing 12%, transient 10%, logging 14%, sensing 6%, actuation 8% and initial energy 1%. We can than represent a histogram of energy consumption sources considers by various models.

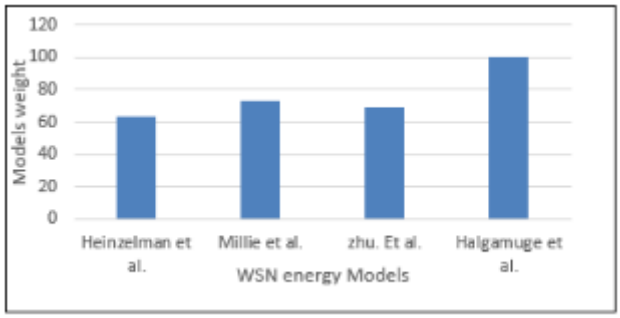

Figure.(15) Different WSN energy consumption Models weight.

2 Simulation Results:
A-Optimal Cluster Number
In order to minimize the energy consumption inside the WSN, sensor nodes must be distributed according to an optimal number of clusters, kopt. And is then obtained by differentiating the total consumed WSN energy with respect to cluster number (k) and setting it to zero. Then, we obtain:

$$\frac{M\sqrt{N}\sqrt{e_{fs}}}{d_{toBS}^{\ 2}\sqrt{2\pi\, e_{mp}}} \quad (9)$$

Next figure (16) shows the dependence of the kopt versus the distance to the base station (dtoBS) or the sink node.

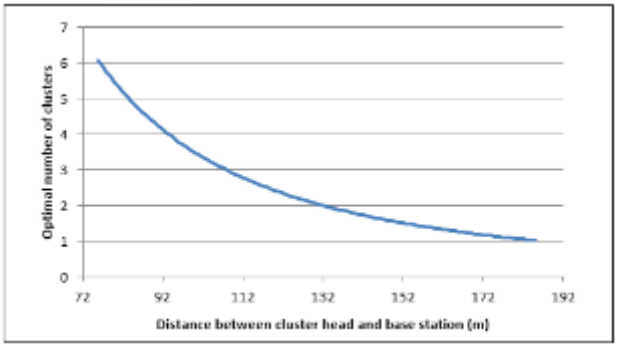

Figure.(16) Optimal number of Clusters vs distance from CH to the sink node (BS) -Analytical results for N=100 nodes, M=100, Efs= 10pJ/bit/m2 and Emp=0.0013pJ/bit/ m4

We can notice that the optimal number of clusters depends strongly on the distance to the base station and reaches the minimum, one cluster, around 190 m. We conclude that this topology (Tree cluster based WSN) is well adapted for small and medium surfaces deployment (residential and industrial units). Moreover, one of the crucial issues in cluster based networks is to determine the optimal number of clusters minimizing the total WSN energy consumption**.**

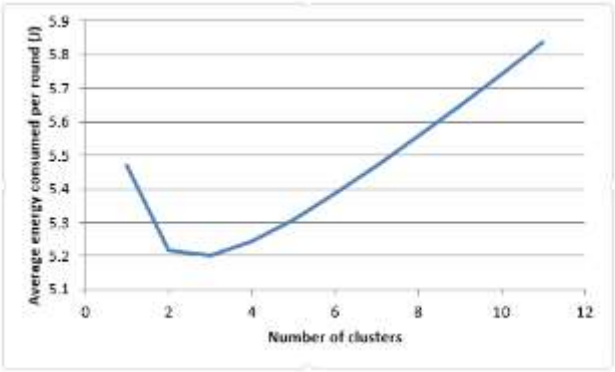

Figure.(17): Average Energy Consumption per round (J) in LEACH when the number of Clusters (k) is varied between 1 and 11.

When varying the number of clusters between 1 and 11, figure (17) shows that optimal number of clusters, kopt, is between 2 and 4.

B- Network lifetime vs Duty Cycle.

Depending on the sensor network topology and the corresponding applications, lifetime is defined as either the time until the first (or last) node dies or the time until a given percentage of nodes dies [25][26]. Duty cycling is a technique where a node is periodically placed into the sleep mode which is an effective method of reducing energy dissipation in wireless sensor networks [27]. The duty cycle expresses the ratio between the time when the node is on and the sum of the times when the node is on and asleep so a DC of 100% is a continuous working node. So it can be expressed by:

$$C_N = \frac{T_{trON} + T_{trOFF} + T_A}{T_{trON} + T_{trOFF} + T_A + T_S} \quad (10)$$

Where TtrON, TtrOFF, TA and TS are time duration respectively to transit from sleep to idle mode, transmit from idle to sleep, active time and sleeping time.

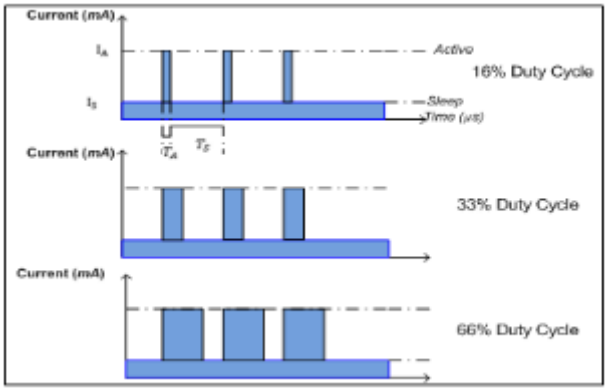

Figure.(18):Duty cycle in expression of the relationship of the "ON time" to "OFF time".

The lifetime of the node depends on the capacity of battery:

$$\text{Node lifetime} = \frac{\textit{initial battery capacity}}{\textit{avg. current} \times 365 \times 24} \text{ [years]} \quad (11)$$

The average current for a sensor node is given by:

$$I_N = C_N \ I_A + (1 - C_N).\ I_S \quad (12)$$

With IA and IS are consumed current during respectively wake up and sleep mode. Next we will present the variation of lifetime of one node as function of the duty cycle which is one of the basic and most commonly used power management techniques

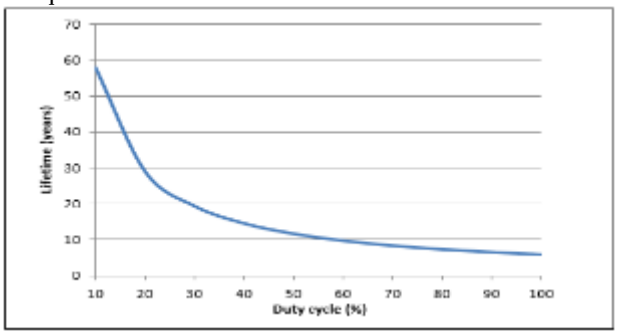

Figure.(19): Sensor node lifetime vs Duty Cycle(%)

The parameter values are taken from Table I and used in equation (10). As the figure (19) shows, when the duty cycle increases the lifetime of the node decreases so we can conclude that lifetime of sensor node is inversely proportional to the duty cycle. Low duty cycle is more appropriate for long lasting WSNs.

C: Average Energy Consumption vs distance from CH to BS:
In WSN, energy has to be managed very carefully in order to increase the network performances. In this section, average energy consumed per round vs the distance from CH to BS (dtoBS) is evaluated. As expected, when (dtoBS) increases, the average energy consumed increases and thus, the WSN lifetime decreases.

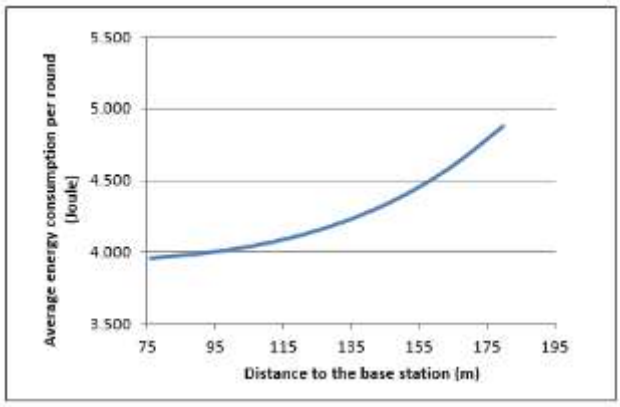

Figure.(20). Average Energy Consumption per round (J) vs distance to the base station.

3 Cloud integration effects on Lifetime and Energy Time dependency:

Sensor Networks have several limitations in terms of energy. Many technics are being developed to save energy in WSN. The most commonly used are data aggregation and processing, Mobile sink for data collection, smart activity scheduling Topology reorganization, data compression, routing protocol [28-30]. Cloud Computing is one of the promising technologies that could help to develop lower energy consumption and longer lifetime in sensor networks. Indeed, when integrating cloud into WSN working process, several shortfalls like data storage capacity and data processing together become much efficient and easier.

A: Cumulative Sensor Node Energy Consumption

Sudip Misra and al. have estimated that a sensor cloud achieves 36.68% decrease in energy consumption, as compared with the case of a classic WSN [31]. In order to better study the behavior of the reduction rate in network energy, we have digitalized figure of "Comparative analysis for energy consumption" using the software Get Data Graph digitizer, from the paper of Sudip Misra et al. [31]. Then we have proceeded to a fitting of both curves "Total expense in sensor cloud" and "Total expense in WSN".

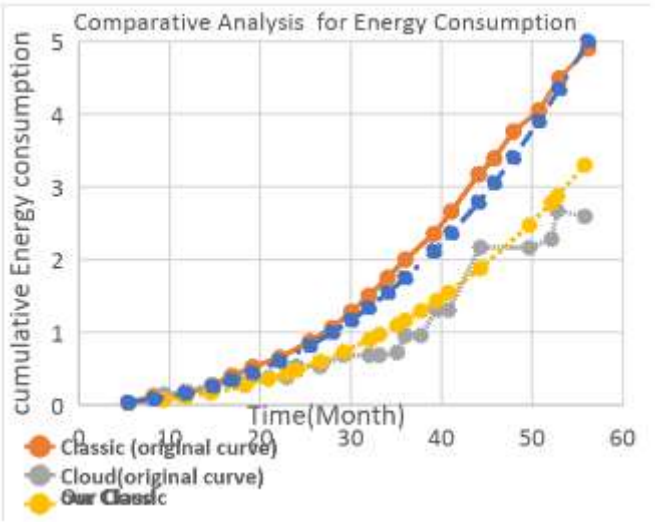

Figure.(21). Cumulative energy consumption vs time (months): (a) curve of reference for classic WSN, (b) curve of reference for cloud WSN, (c) curves obtained by fitting for classic WSN, (d) curves obtained by fitting for cloud WSN.

When fitting, we can notice that next equation tie in to the curve of cloud computing WSN energy consumption

$$F(x)= \frac{x}{6} \log\left(\frac{1}{1-\frac{x}{100}}\right) \quad (13)$$

And this one tie in to the curve of classic WSN energy consumption:

$$f(x)= \frac{x}{4} \log\left(\frac{1}{1-\frac{x}{100}}\right) \quad (14)$$

$$G_E = \left| \frac{E_{wsn\,classic} - E_{wsn\,cloud}}{E_{wsn\,classic}} \right| * 100\% \quad (15)$$

Where Ewsn classic and Ewsn cloud are are respectively cumulative energy consumption in a classic WSN and in a cloud WSN. We can than conclude that the gap of energy, estimated from the fitting equation, is constant in time and equal to 42.8% compared to 36.68% on Sudip Misra work.
Next table illustrates the amelioration in sensor node power consumption with cloud integration.

Working Mode	*Current Consumtion Before Cloud*	*Current Consumption after Cloud.*
Sleep	1µA	0.58 µA
Wakeup	8mA	4.64 mA

B- Sensor Node Lifetime Reduction Rate
As the energy consumed in the sensor network decrease by integrating cloud, this will affect also the sensor node lifetime. Sudip Misra et al. estimated that sensor cloud increases the lifetime by 3.25% [31]**.** In order to better study this increase in lifetime, we have digitalized figure 7 titled "Comparative analysis of sensor node lifetime" from the paper of Sudip Misra et al. [31]. Figure (22) illustrates a comparative analysis of sensor Node lifetime reduction rate.

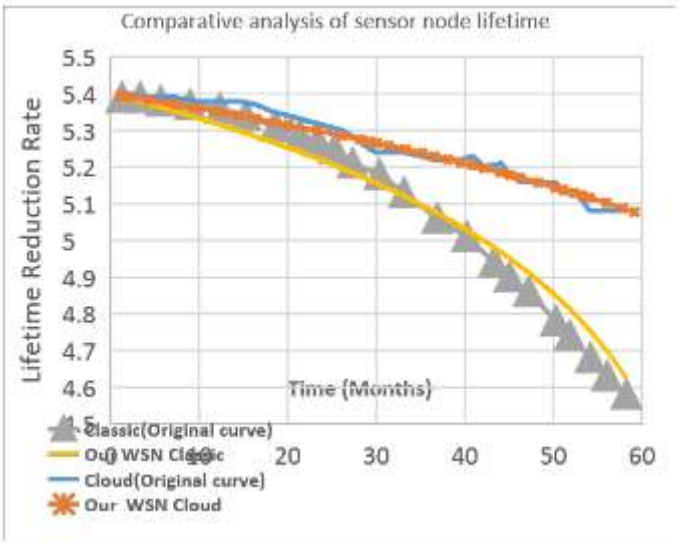

Figure.(22). Lifetime reduction Rate vs time (months): (a) curve of reference for classic WSN, (b) curve of reference for cloud WSN, (c) curves obtained by fitting for classic WSN, (d) curves obtained by fitting for cloud WSN.

Thanks to a logarithmic fitting, the sensor node lifetime on a classic network can be expressed as follow:

$$z(x) = 5.4 + \log(1 - \frac{x}{70}) \quad (16)$$

And a sensor node lifetime in a cloud computing network can be expressed as follow:

$$Z(x) = 5.4 + \log(1 - \frac{x}{113}) \quad (17)$$

In Fig. 22, we depict the reduction rate between classic and cloud WSN sensor node operation period (lifetime) where the reduction rate is expressed as follows:

$$G_L = \left| \frac{L_{wsn\,classic} - L_{wsn\,cloud}}{L_{wsn\,classic}} \right| * 100\% \quad (18)$$

In this graph, we can evaluate the gap at any point of time during 60 months.

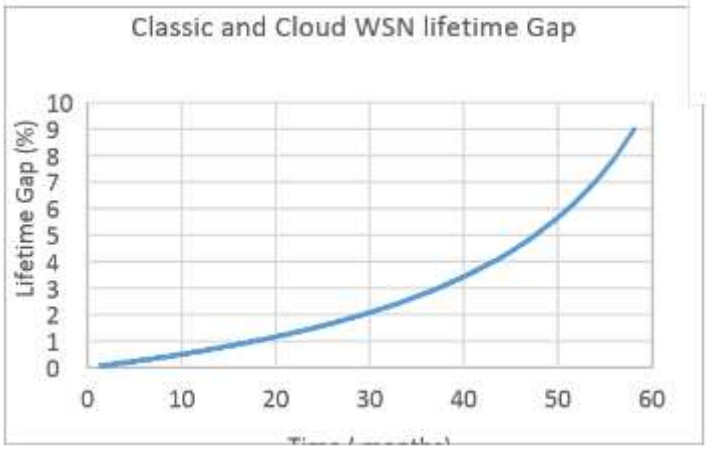

Figure.(23). Lifetime Gap vs Time

Based on the logarithmic equation, the average lifetime reduction rate during 60 months is 3% compared to 3.25% on the Sudip Misra Work.

Dimensionning of photovoltaic harvester to supply a sensor node

1. Indoor Light Estimation

Amorphous silicon (a-Si) PV cells have a relatively high efficiency at low light levels, compared to other types of cell. This makes them particularly suited to use indoors. In most cases, a solar cell panel consists of multiple solar cell elements connected in parallel and/or series, where the current source of the solar cell is dependent on the intensity of the incident light.

Since the light is estimated to be available only for 8 hours and the sensor operates all day, then the output of PV cell power should be greater than power consumed by the node on the active mode multiplied by 4.64mA*24h/8h.

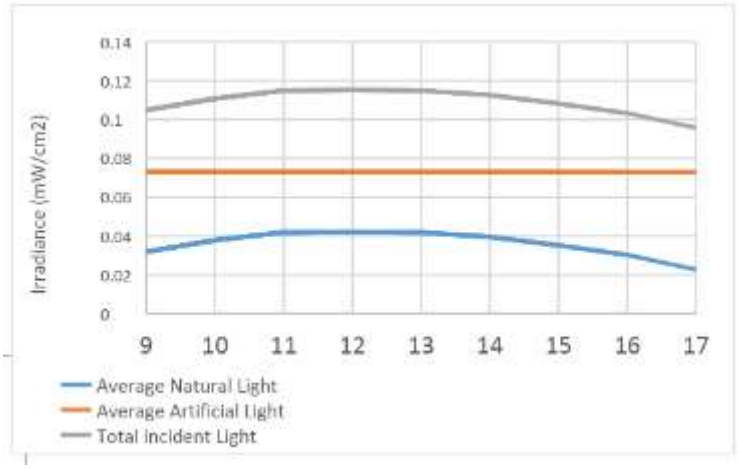

Figure.(24).. natural and artificial simulated indoor light irradiance from 09:00 AM to 05:00PM.

Photovoltaic harvesting is a promising energy source because of the available irradiance both indoors and outdoors **[33-34].** We consider that the sensor consumes 4.9 mWh/day **[35].**

The amorphous silicon solar cell was judged as the most suitable cell for indoor conditions in terms of efficiency reaching 18% for 0.172 mWh/cm2 **[36]** of averaged energy delivered. The sensor with an energy consumption of 4.9 mW/h/day could thus be powered with an amorphous silicon solar cell with an area of 28.3 cm2.

Table IX. energy and power densities from a solar cell

Average WSN energy consumption **(mWh/day)**	***Irradiance*** **(mW/cm2)**	***hours***	***Average Power generated*** **(mWh/cm2)**	***Cell surfaces*** **(cm2)**
4.9	0.12	8	0.172	28.3

Amorphous-silicon and dye-sensitized solar cells have been tested extensively as indoor light harvesters due to their wide bandgaps that are optimum for absorption of the spectra from compact fluorescent lamp (CFL) and light-emitting diode (LED) bulbs **[37].** An additional feature of amorphous silicon (and, indeed, all noncrystalline) PV cells is that their MPP voltage (Vmpp) is approximately proportional to their open-circuit voltage (Voc).

In [38], the author adopted an a-si 55mm x40mm Sanyo AM1815/16 module series PV cell and in [39] they used a Schott Solar 1116929 amorphous silicon PV cell placed on an office desk under 200-700 lux and the size of the adopted PV modules is greater than 20cm.

Our presented credit card-sized indoor series connected photovoltaic energy harvester (less than 80 mm × 50 mm) supplies 1 mW to the WSN mote when the PV cell is under 700–800 lux indoor light in a typical office building environment. Larger PV cells provide higher charging currents but that implies oversized harvesting system.

2. MPPT command : the Fractional open circuit Voltage

There are so many MPPT techniques that have been already proposed in the literature; for example the Perturb and Observe (P&O), the Incremental Conductance (IC), Fractional open-circuit voltage (FVOC), fractional short circuit current (FSC), Neural network, Fuzzy logic control, etc. Our approach is to avoid the use of the

MCU and utilize the FVOC method. The simple computation and low power consumption make this MPPT method suitable for small-scale PV devices.

Low-frequency MPPT is adopted in this work in order to reduce the switching loss on the MOSFET. This MPPT converter operates in discontinuous conduction mode with lower inductor current. The MPPT Pulse Width Modulation (PWM) control signal is generated from the analog comparator. A reference PV cell made from the same technology as the main PV cell is used as the voltage reference. Instead of disconnecting the PV cell to measure the VOC, the pilot PV cell provides a reference VOC which is proportional to the open circuit voltage of the main PV cell. This method further reduces the complexity and power consumption of the MPPT controller.

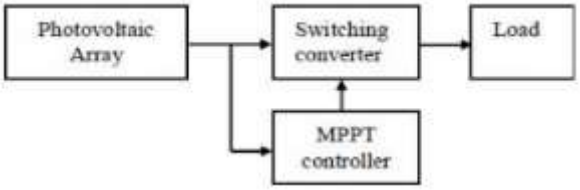

Figure.(25). General System Architecture

The reference PV cell is not connected and insure the measurement of the Voc, next figure show the Matlab simulation of the Voc and Isc of the Cell, the cell take 4.10-4 second to stabilize and reach 0.6015 V.

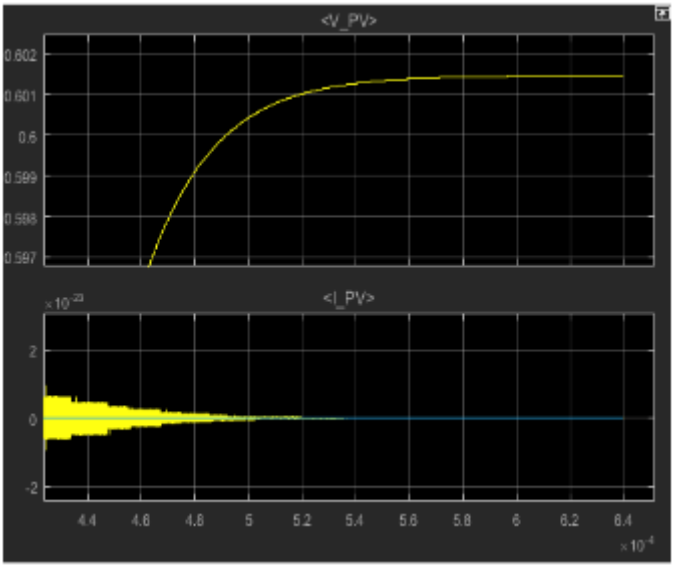

Figure.(26). Secondary PV cell Current and voltage stabilization

The problem considered by MPPT is to automatically find the operating point (Vpv, Ipv) at which a PV module should operate to obtain the maximum output power under a given temperature and irradiance, following it when light intensity changes. In our case we adopt the FVoc method for tracking the maximum power point on which the PV cell should always operates, this method has shown good efficiency in indoor conditions and is known by the proportionality between the MPP and the cell Voc expressed as follow:

$$V_{MPP} = K * V_{oc}$$

$$V_{oc} = \frac{\eta K T}{q} ln\left(\frac{I_L}{I_0} + 1\right)$$

This relationship is exploited by some MPP circuits, which periodically sample the open-circuit voltage of the PV cell in order to decide its activity level. The asset of this ultra-low-power MPPT system is that it can cold start and operate in a very wide range of lighting conditions including the low intensities found indoors. From our simulation results:

Table X. The factor K in function of light intensity.

Intens. (lux)	Voc	Vmpp	k
100	0.583947	0.40972	0.701639
200	0.610053	0.429524	0.704077
300	0.625324	0.441109	0.705409
400	0.636159	0.449329	0.706315
500	0.644563	0.455704	0.706997
600	0.651429	0.460913	0.707541
700	0.657235	0.465318	0.707993
800	0.662264	0.469133	0.708377

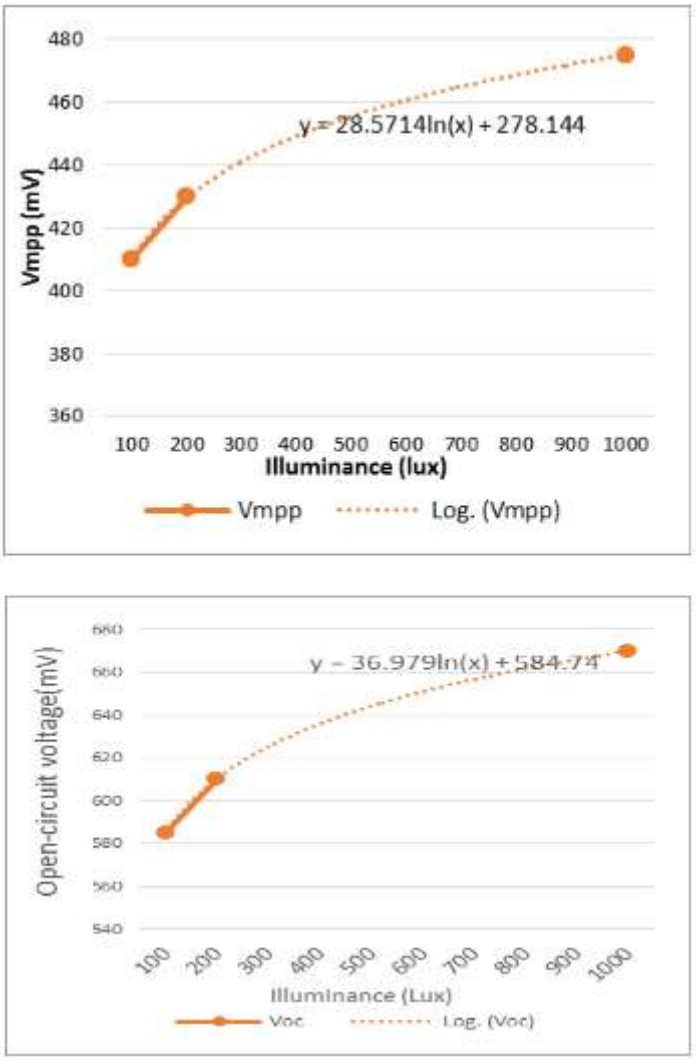

Figure.(27). (a) PV cell voltage at maximum power point vs light illuminance. (b) Open circuit pv cell voltage vs ligh illuminance.

Some researchers consider the factor K as a set of constants ranging from 0.71 to 0.78, depending on the photovoltaic panels material characteristics and illuminance conditions [40]. In this study and from this simulation, the factor k will be set to 0.708.

3. Boost converter

Commonly used power electronics converters for the MPP systems are either buck converter, boost converter or buck-boost converter. However, the boost converter is commonly used in PV based applications. As it has some advantages over the other converters as it is more stable and efficient. The Synchronized Boost Converter MPPT consists of two main building blocks: tow Comparators based MPPT controller and synchronous boost converter.

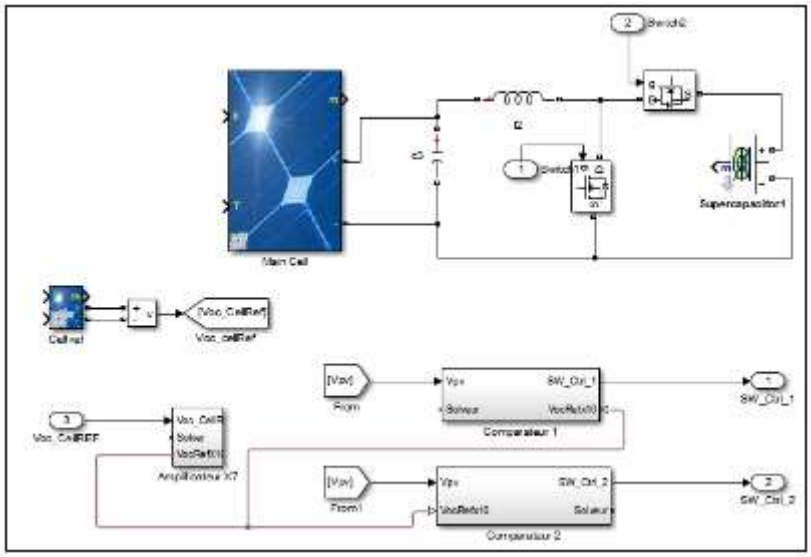

Figure.(28).Schematics of Maximum Power Point Tracking

Each switch is controlled by a comparator. In switch ON mode the switch is in conducting mode and whole current will follow the resistance free path through the switch. So, the diode will act as an open circuit. So that the inductor will be energized. The energizing of the inductor is dependent on the ON-OFF switching time.

In switch OFF mode, the switch will open and whole current will flow through the diode that will now act as a short circuit. The voltage produced by the inductor during its energizing in Switch ON mode will release in Switch OFF mode.

Table XI. Components parameters of Boost Converter

C input resistance	1e-3 Ω	I avg Load	0.00155 mA
C input capacitance	1e-9 F	V supply load	2.7 V
C out capacitance	5F	R load	174 103Ω
C out Resistance	1e-3 Ω	R inductor	1e-3 Ω
Inductor capacitance	1e-4 H		

4. Testing of Maximum Power Point Tracking

A Matlab model is created to simulate the boost converter MPPT. The captured simulation results show two cycles of the power tracking process in next Figure.

In this case, the PV cell voltage will oscillate around V_{MPP} and $V_{MPP} = K * Voc * n = 2.55$ V.

Hysteresis is adopted in the design to switch on transistor SW1 when input capacitor voltage (PV cell voltage) is higher than $V_{MPP} + \frac{V_{hyst1}}{2}$. We set the V_{hyst1} to 0.2 V and V_{hyst2} to 0.4V and the only condition

when choosing those values $V_{hyst1} < V_{hyst2}$. The hysteresis can be easily adjusted by scaling the resistors in both comparator and time ON is between t_0 and t_1.

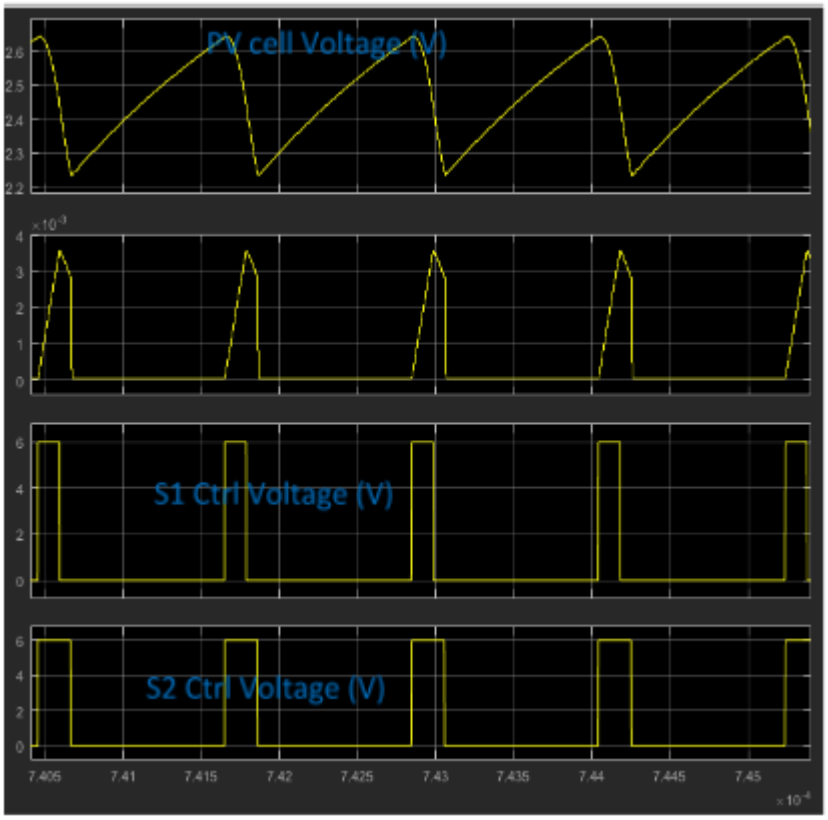

Figure.29.Boost converter Matlab simulation and control signals of switch 1 and switch 2.

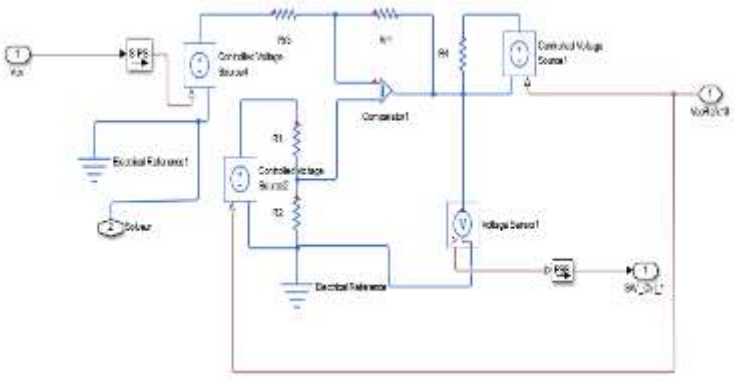

Figure.30. Switch 1 'Comparator

The hysteresis voltage is described in the equation below:

$$V_{hyst} = V_{UPP} - V_{low} = \frac{R_1}{R_2} * V_{oc}$$

Where:

$$V_{UPP} = \frac{R_1+R_2}{R_2} * V_{ref}$$

$$V_{low} = \frac{R_1+R_2}{R_2} * V_{ref} - \frac{R_1}{R_2} * V_{oc}$$

$$V_{cc} = V_{oc} * n$$

The input capacitor is then discharged whilst the inductor L is charged with variable current IL(t). once the capacitor voltage drops toVMPP- Vhyst12, the SW1 is turned off due to the hysteresis, the ON stage time is from t0 to t1. Next table presents the resistance values for both comparators.

Table XII: resistance values of first comparator

R1= 100 MΩ	**Rr3= 100 MΩ**	**R4= 1 KΩ**
R2= 242465753 Ω	**Rr1= 3004988280 Ω**	

Table XIII: Resistance values of second comparator

R8= 188,7 MΩ	**R3= 1 KΩ**	**Rr= 1 KΩ**
R9= 412,2 MΩ	**R7= 15 KΩ**	

Hysteresis voltage Vhyst2 is also set by the comparator resistor array.

5. Energy Storage Unit

In [41] Brunelli et al. presented a system with a 50 F supercapacitor as the only energy storage device. The PWM-controlled MPPT circuit implements the fractional open circuit voltage method. The carefully simulated and implemented MPPT sub-system only requires mW-level power consumption. In our design we use a supercapacitor as an energy storage unit (ESU) with 5F capacitance and 3V initial voltage.

The power management unit is essentially composed of boost converter based on an inductor and two switch and an input capacitor with a capacitance of 3µF and an internal resistance of 1mΩ. We suppose that the initial state of the input capacitor is discharged, the PV cell is going to charge it, next figure is the charging curve of the input capacitor.

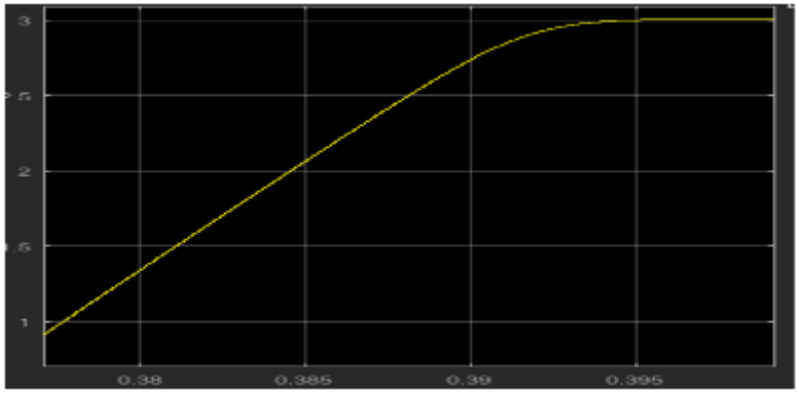

Figure.31. Voltage (V) vs time (ms)

When the input capacitor reaches a voltage reference Vcap-max set to 3V in this study, the transistor S1 is switched ON and the input capacitor started to discharge while the input inductor starts to be charged with

variable current IL(t). From the simulation, 0.3ms are needed to charge the input capacitor from 1V to 3V. Once the capacitor voltage drops to Vcap-min, the SW1 is turned off.

6. The three studied scenarios

The objective of this section is to compare three designs of the boost converter-based FVOC MPPT method which are presented in next figure.

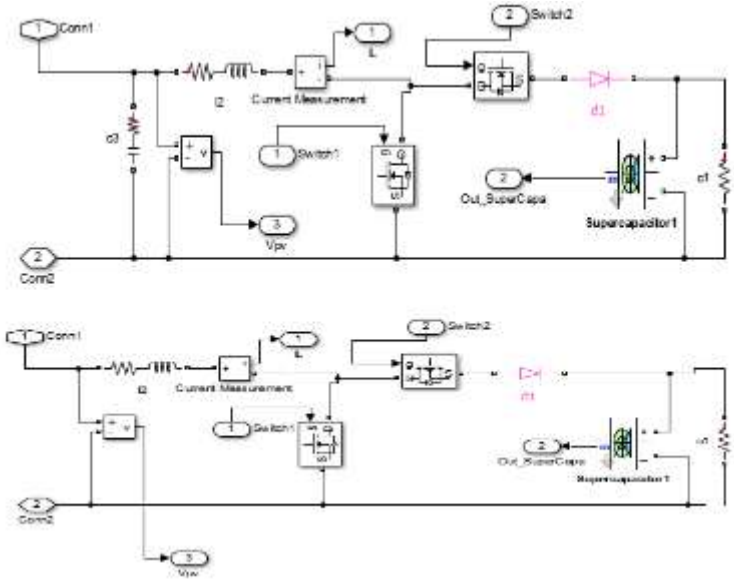

Figure. 32. (a)First scenario: boost converter with input capacitor. (b)Second scenario: Boost converterwithout input capacitor. (c)Third scenario: direct connection without MPPT command.

The three scenario are made using Matlab, the direct connection consists of connecting the cell directly to the energy storage unit and inserting only a diode while the only difference between the first and second scenario is the use of the input capacitor. Voltage in direct connection is constant and voltage in first and second scenario is estimated to be around:

V= K*Voc*n = **0.708 *0.601* 6 = 2.55 V**

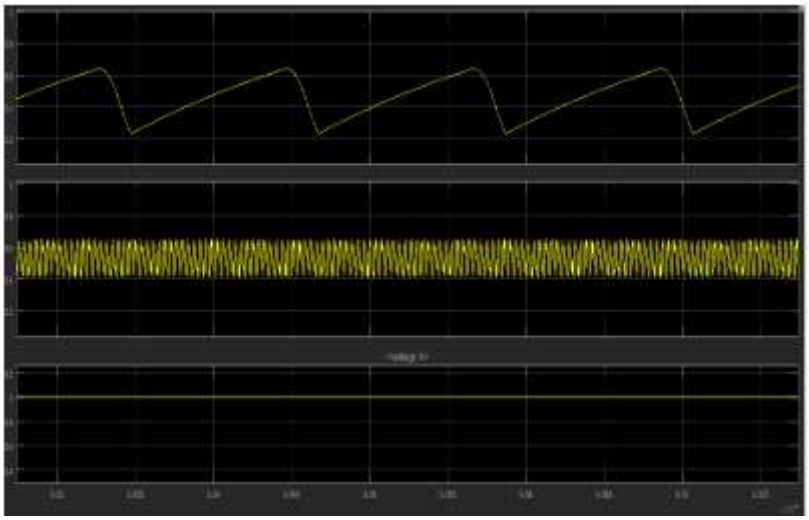

Figure. 33. PV cell voltage connected to (a): Boost converter with input capacitor. (b): Connected to a Boost converter without input capacitor. (c): directly connected to the load.

Previous PV module voltage plots shows that the frequency is very high when not using an input capacitor. High frequency influences the performance and the stability of the boost converter. We can confirm that integration of input capacitor in the boost converter reduces the power loss in an MPPT circuit and impacts on the system conversion efficiency. The voltage frequency analysis helps us to decide that first scenario is more stable than the second. We are going to change the number of series connected PV cell and study the SoC of the supercapacitor for each scenario, results are shown in next table.

Table XIV: SoC of the output capacitor vs the number of series connected PV cells for three different system scenarios.

scenario	*Number of serie PV cells*	*State of Charge (2000s)*
First scenario	*1*	**0.23%**
	6	**2%**
	10	**6%**
Second scenario	*1*	**0.26%**
	6	**2%**
	10	**4%**
Third scenario	*1*	**No charging**
	6	**2.8%**
	10	**5%**

The SoC was calculated during 2000 second. We can conclude that the more we have a series connected PV cells the more the charging speed is higher and one the voltage delivered by the module is higher than the initial voltage of the SC than the system will no longer need a boost converter to increase voltage. A six series connected PV cells in the direct connection gives a better charging speed than both other scenarios.

Conclusion

We used simulations to study the characteristics of indoor electrical artificial and natural light in a typical office in Tunisia.

The majority of inside light study are looking for reducing building's energy consumption while this paper presents a novel exploitation method using Dialux software for estimating the amount of natural and electrical artificial indoor light and its characteristics in order to supply a sensor node. The research question of this study is where the optimal PV panel position is, to avoid the light nonuniformity phenomenon and mostly to well know the indoor light distribution.

In this work, we showed that the cluster based WSN with 3 clusters and 100 nodes is suitable for residential and professional use, spread on near 100 m square areas. In such a configuration, the used energy consumption model is based on the major consuming component related to communication and processing. We showed also that the integration of Cloud computing in the WSN applications decreases, the energy consumption by 42.8% and increases the lifetime by 3%.

In means of conclusion, the results of our study are strongly related to our assumptions, the artificial and natural light in our case do satisfy the visual comfort conditions on a working place and also could supply a sensor node.

The presented credit card-sized indoor photovoltaic energy harvester (4cmx5cm) supplies 0.15 mWh/cm2 regulated power to the WSN mote when the solar cell is under 300–800 lux indoor light. This generated power is sufficient for low duty cycle (0.1% or less) using the selected WSN mote. It met the final target of long-term WSN power autonomous operation in a typical office/residential building environment.

A design of three scenarios of power management circuit for light harvesting to supply a WSN were presented. Those design was extensively simulated and analyzed. The proposed simulation was analyzed and validated by extensive simulation results. It was proved that it can precisely estimate maximum power point voltage.

As it was proved, the use of input capacitor is essential for better stable module voltage, then the second scenario is better than the first. For the third scenario, we can choose to work with a direct connection if the PV module supplies a voltage higher than the initial state voltage of the output capacitor and this is depending of the number of series connected PV cells.

In this paper, the concept of using the fractional voltage open circuit (FVOC) method in the sub 1 mW MPPT design for its superior ultra-low power consumption was proved to be feasible, and the implementation is suitable for WSN applications.

The presented credit card-sized indoor photovoltaic energy harvester supplies 0.2 mW–0.4 mW regulated power to the WSN mote when the solar cell is under 500–800 lux indoor light. This generated power is sufficient for low duty cycle (0.1% or less)

References

[1] k. Ruhle,. S.W Glunz,. ; M.Kasemann, "Towards new design rules for indoor photovoltaic cells" Dept. of Microsyst. Eng., Univ. of Freiburg, Freiburg, Germany. 2011
[2] W. Maranda, M.Piotrowics, Departerment of Microelectronics and computer science,Technical university Lodz.Mixedes 2011, 18th international conference "Mixed design of integrated circuits and systems" June 16-18,2011.
[3] Y. Afsar, J. Sarik, M. Gorlatova, G. Zussman, l. Kymissis, "Evaluating photovoltaic performance indoors", in: 2012 38th IEEE Photovoltaic Specialists Conference (PVSC), pp. 19481951, 2012.
[4] Qiu, Yifeng; Van Liempd, Chris; het Veld, Bert Op; Blanken, Peter G; Van Hoof, Chris "5µW to10mW input power range inductive boost converter for indoor photovoltaic energy harvesting with integrated maximum power point tracking algorithm" SolidState Circuits Conference Digest of Technical Papers (ISSCC), 2011 IEEE International , Issue Date: 20-24 Feb. 2011.
[5] Karola Ruhle, Martin Kasemann "Selection and dimensioning of photovoltaic harvester for wireless sensor systems" Sensoren und Messsysteme 03. – 04.06.2014 in Nürnberg.
[6] Alex S. Weddell, Member, IEEE, Geoff V. Merrett, Member, IEEE, and Bashir M. Al-Hashimi, Fellow, IEEE "Photovoltaic Sample-and-Hold Circuit Enabling MPPT Indoors for Low-Power Systems" IEEE Transactions ON Circuits AND Systems—I: REGULAR PAPERS, VOL. 59, NO. 6, JUNE 2012
[7] Yin Li and Ronghua Shi "An intelligent solar energy-harvesting system for wireless sensor networks" Li and Shi EURASIP Journal on Wireless Communications and Networking179 DOI 10.1186/s13638-015-0414-2. 2015
[8] 6ème enquete aupres des clients , direction des etudes et de la planification residentiels de la STEG 2009.
[9] Dialux 4 with new improved calculation kernel. http://www.dial.de/DIAL/fileadmin/download/dialux/wissen/Dx4_Rechenkern_eng.pdf
[10] G. Anastasi, M. Conti, M.D. Francesco, A. Passarella, "Energy conservation in wireless sensor networks": a survey, Ad Hoc Networks Journal 7 (3) (2009) 537–568.
[11] M. N. Halgamuge, M. Zukerman, and K. Ramamohanarao "AN ESTIMATION OF SENSOR ENERGY CONSUMPTION" Progress In Electromagnetics Research B, Vol. 12, 259–295, 2009
[12] Wendi B. Heinzelman, Anantha P. Chandrakasan, and Hari Balakrishnan, "An Application-Specific Protocol Architecture for Wireless Microsensor Networks" IEEE TRANSACTIONS ON WIRELESS COMMUNICATIONS, VOL. 1, NO. 4, OCTOBER 2002
[13] Vintesh Patel, Bintu Kadhiwala "Integration of Wireless Sensor Network with Cloud Computing" submitted in Partial Fulfilment of the Requirement for the Award of Degree of Master of Engineering in Computer Engineering. Published on Oct 19, 2013
[14] Wendi B. Heinzelman, Anantha P. Chandrakasan, and Hari Balakrishnan, "An Application-Specific Protocol Architecture for Wireless Microsensor Networks" IEEE TRANSACTIONS ON WIRELESS COMMUNICATIONS, VOL. 1, NO. 4, OCTOBER 2002
[15] M. N. Halgamuge, M. Zukerman, and K. Ramamohanarao "An Estimation of Sensor Energy Consumption" Progress In Electromagnetics Research B, Vol. 12, 259–295, 2009

[16] M. N. Halgamuge, M. Zukerman, and K. Ramamohanarao "An Estimation Of Sensor Energy Consumption" Progress In Electromagnetics Research B, Vol. 12, 259–295,
[17] Amin Rostami and Mohammad Hossin Mottar "Wireless Sensor Network Clustering Using Particles Swarm Optimization For Reducing Energy Consumption" International Journal of Managing Information Technology (IJMIT) Vol.6, No.4, November 2014.
[18] Qin Wang, Mark Hempstead and Woodward Yang "A Realistic Power Consumption Model for Wireless Sensor Network Devices" 3rd Annual IEEE Communications Society on Sensor and Ad Hoc Communications and Networks- 28 Sept. 2006.
[19] Wendi B. Heinzelman, Anantha P. Chandrakasan, and Hari Balakrishnan, "An Application-Specific Protocol Architecture for Wireless Microsensor Networks" IEEE TRANSACTIONS ON WIRELESS COMMUNICATIONS, VOL. 1, NO. 4, OCTOBER 2002
[20] Priya Gupta1, Ruchita Gupta1, Shikha Ranjan1, R.N.Shukla2 "Wireless Sensor Network (WSN) simulation framework using MatLab software" International Journal of Electronics, Electrical and Computational System IJEECS ISSN 2348-117X Volume 3, Issue 4,June 2014
[21] MATLAB Web Site: http://www.mathworks.com/
[22] Mille, M. J. and N. H. Vaidya, "A mac protocol to reduce sensor network energy consumption using a wakeup radio," IEEE Trans. Mobile Computing, Vol. 4, No. 3, 228–242, May 2005.
[23] Rabia Enam , Mumtazul Imam , Rehan Qureshi "Energy consumption in Random Cluster Head selection Phase of WSN"
[24] Pengfei Zhang , Gaoxi Xiao , Hwee-Pink Tan "Clustering algorithms for maximizing the lifetime of wireless sensor networks with energy-harvesting sensors" Computer Networks 57 (2013) 2689–2704.
[25] Dong, Q., "Maximizing system lifetime in wireless sensor networks," Proc.IEEE Int.Symp.Info.Processing in Sensor Networks Conf., 13–19, Apr. 2005.
[26] Jyoti Saraswat, Partha Pratim Bhattacharya "Effect OF Duty Cycle ON Energy Consumption IN Wireless Sensor Networks" International Journal of Computer Networks & Communications (IJCNC) Vol.5, No.1, January 2013
[27] C. Chen, B. Tian, Y. Li, and Q. Yao, "Data aggregation technologies of wireless multimedia sensor networks: a survey," in 2010 IEEE International Conference on Vehicular Electronics and Safety (ICVES), 2010, pp. 83-88.
[28] X. Zhe-yuan, F. Xiao-ping, L. Shao-qiang, and Z. Zhi, "Distributed image coding in wireless multimedia sensor networks: a survey," in 2010 Third International Workshop on Advanced Computational Intelligence (IWACI), 2010, pp. 618-622.
[29] T. Ma, M. Hempel, D. Peng, and H. Sharif, "A survey of energy efficient compression and communication techniques for multimedia in resource constrained systems," Communications Surveys & Tutorials, IEEE, vol. PP, 2012, pp. 1-10.
[30] S. Ehsan and B. Hamdaoui, "A survey on energy-efficient routing techniques with QoS assurances for wireless multimedia sensor networks," Communications Surveys & Tutorials, IEEE, vol. 14, 2012, pp. 265-278.
[31] Sudip Misra, Subarna Chatterjee, Mohammad S. Obaidat "On Theoretical Modeling of Sensor Cloud: A Paradigm Shift From Wireless Sensor Network" IEEE Systems Journal,20 November 2014
[32] "Addressing the Challenges of Power Management in Wireless Sensor Networks (WSNs)" By European Editors Contributed By Digi-Key's European Editors 2013-07-16.
[33] I.F. Akyildiz, W. Su, Y. Sankarasubramaniam, and E. Cayirci. "Wireless sensor networks: a survey". Computer Networks, 38(4):393–422, March 2002.
[34] Abhiman Hande, Todd Polk,WilliamWalker, and Dinesh Bhatia. "Indoor solar energy harvesting for sensor network router nodes". Microprocessors and Microsystems, 31(6):420–432, September 2007.
[35] Karola Ruhle, Martin Kasemann "Selection and dimensioning of photovoltaic harvester for wireless sensor systems" Sensoren und Messsysteme 03. – 04.06.2014 in Nürnberg.
[36] Y. Afsar, J. Sarik, M. Gorlatova, G. Zussman, l. Kymissis, "Evaluating photovoltaic performance indoors", in: 2012 38th IEEE Photovoltaic Specialists Conference (PVSC), pp. 19481951, 2012.
[37] Ian Mathews, Paul J. King, Frank Stafford, and Ronan Frizzell "Performance of III–V Solar Cells as Indoor Light Energy Harvesters" IEEE JOURNAL OF PHOTOVOLTAICS.

[38] Issa Jafer , Paul Stack and Kevin MacNamee. School of Engineering, University College Cork, Western Road, Cork, Ireland. "Design of New Power Management Circuit for Light Energy Harvesting System". Sensors 2016, 16(3), 270.
[39] Alex S. Weddell, Geoff V. Merrett, Bashir M. Al-Hashimi School of Electronics and Computer Science, University of Southampton, SO17 1BJ, UK "Ultra Low-Power Photovoltaic MPPT Technique for Indoor and Outdoor Wireless Sensor Nodes"
[40] B.M Hasaneen "Design and Simulation of DC/DC Boost Converter," IEEE 12th International Middle East Power System Conference (MEPCON), pp. 335 – 340, 2008. [8] W. Xiao, N. Ozog, W.G. Dunford, "Topology Study of Photovoltaic Interface for Maximum Power Point Tracking" IEEE Transactions on Industrial Electronics, vol. 54, pp. 1696 – 1704, June 2007.
[41] Brunelli, D.; Moser, C.; Thiele, L.; Benini, L. "Design of a Solar-Harvesting Circuit for Battery-less Embedded Systems ". IEEE Trans. Circuits Syst. I: Regul. Pap. 2009, 56, 2519–2528.